Compaction performance of a scale model vibrating drum roller on lunar highlands regolith simulant

Akshay K. Agarwal,[1] Brendan T. Scott, Ph.D.,[1] and Mark B. Jaksa, Ph.D.[1]

[1]School of Civil Engineering and Construction Management, Adelaide University, SA, 5005, Australia; e-mail: akshaykumar.agarwal@adelaide.edu.au

ABSTRACT

As NASA is progressing towards crewed long-term missions to the lunar South Pole, a detailed understanding of the geotechnical behaviour of lunar highlands regolith will be essential for the design of foundations, mobility systems, and in situ construction processes. This study investigates the compaction behaviour of a lunar highlands regolith simulant using a scale model lunar vibrating drum roller (LVDR-1). Two drum roller masses—2.92 kg and 4.45 kg—were examined under controlled vibration frequencies and translational scale speeds. For the 2.92 kg mass, scale speeds of 2 km/h and 4 km/h were tested at 40 Hz and 30 Hz, respectively, whilst for the 4.45 kg mass, scale speeds of 2 km/h and 6 km/h were tested at 40 Hz to evaluate their influence on compaction performance. Key parameters, including surface settlement, vertical pressure, penetration resistance, and bulk density, were recorded to assess the effectiveness of each roller configuration. The results show that the heavier roller mass consistently provides superior compaction performance, achieving greater surface deformation, higher penetration resistance, increased bulk density, and deeper stress transmission within the simulant bed.

KEYWORDS: lunar construction, lunar infrastructure development, vibrating smooth drum roller, mass, frequency, speed.

1. INTRODUCTION

The Artemis program aims to establish a sustainable human presence on the lunar surface, enabling future space exploration and in situ resource utilisation. Achieving this objective requires the development of essential infrastructure on the lunar surface, including roads, habitats, and spaceports. A critical step in this process is enhancing the stability and load-bearing capacity of the lunar surface to ensure that it can support long-term habitation and operational activities. One of the promising approaches to achieving this objective is lunar surface compaction. This process involves the densification of lunar regolith by reducing the void ratio and enhancing particle interlocking, thereby improving its load-bearing capacity, shear strength and overall mechanical properties, which are essential for the long-term stability of lunar infrastructure (Das and Sobhan, 2014; Dotson et al., 2024; Terzaghi et al., 1996).

As humanity advances towards establishing a sustained presence on the Moon, an understanding of lunar regolith behaviour under engineered operations becomes a

fundamental necessity for the design and development of lunar surface infrastructure and mobility systems. The geotechnical characteristics of lunar soil, particularly the highland regolith prevalent in the lunar south polar region, dictate the feasibility of surface mobility, infrastructure development, and in situ resource utilisation. These characteristics influence the performance of engineering systems such as foundations, transportation routes, and construction platforms required for long-term lunar operations.

Agarwal et al. (2023) demonstrated that LHS-1E, an engineering-grade lunar highlands simulant manufactured by Space Resource Technologies, exhibits geotechnical properties and mechanical behaviour closely aligned with actual lunar highlands regolith (Carrier et al., 1991; Dotson et al., 2024). This validation provided a foundation for safe and scalable Earth-based testing environments. In addition, Agarwal et al. (2024) reviewed various regolith compaction techniques and evaluated their suitability for lunar surface construction, identifying both vibrating smooth drum roller (VSDR) and rolling dynamic compaction (RDC) as promising techniques for extraterrestrial ground improvement.

Extending this line of research, Agarwal et al. (2026a) experimentally investigated these two distinct compaction techniques for their efficacy on LHS-1E simulant. The findings emphasised that VSDR provides superior surface densification and deeper influence zones compared to RDC. In a subsequent study, Agarwal et al. (2026b) varied operational parameters to analyse the effects of roller speed, motor frequency and drum roller mass. Two configurations, 2 km/h at 40 Hz for a 2.92 kg mass, and 6 km/h at 40 Hz for a 4.45 kg mass, demonstrated the greatest promise and warranted further investigation.

This study conducts a targeted, comparative investigation of the two aforementioned configurations to assess their relative compaction performance under controlled laboratory conditions, focusing on metrics such as surface density, penetration resistance, and vertical pressure. Additionally, vertical acceleration responses were analysed for different mass and frequency configurations to better understand roller dynamics.

2. BACKGROUND

Compaction is a fundamental ground improvement process that enhances the load-bearing capacity of soil and reduces settlement through particle rearrangement, void reduction, and, in some cases, particle breakage (Terzaghi et al., 1996). While terrestrial soil compaction typically involves mechanical processes such as static, dynamic, impact, and vibratory loading to reduce air voids, the compaction behaviour of lunar regolith is expected to differ significantly due to the absence of air and water, reduced gravity, and the unique environment of the Moon, including vacuum conditions, extreme temperature variations, and regolith particle angularity (Agarwal et al., 2024; Bernold, 1994; Carrier et al., 1991).

Agarwal et al. (2024) provided a comprehensive review of six terrestrial ground improvement techniques—deep dynamic compaction, rapid impact compaction, vibrating plate compactors and rammers, smooth drum rollers, vibrating smooth drum rollers (VSDRs), and RDC and evaluated their potential applicability under lunar conditions. Their analysis identified RDC and VSDRs as the most promising candidates for extraterrestrial applications.

Building on this foundation, Agarwal et al. (2026a) conducted a comparative experimental study between scale models of a four-sided impact roller (i.e. RDC) and a

VSDR. The results demonstrated that the VSDR achieved greater surface settlement, higher peak stresses, increased density, and a deeper zone of influence than the impact roller, highlighting the superior suitability of vibratory compaction for lunar application. In a subsequent study, Agarwal et al. (2026b) systematically varied operational parameters to investigate the influence of roller speed, motor frequency, and drum roller mass on compaction performance. This work provided quantitative data on surface settlement and stress transmission, offering valuable insights into how different operational conditions affect the efficiency of lunar highlands regolith simulant compaction. Despite extensive investigations of VSDR performance in terrestrial contexts, research addressing extraterrestrial environments remains limited. Wersäll (2016) emphasised the significance of vibration frequency in controlling soil compaction outcomes, underscoring the need for systematic investigations of vibratory loading effects on lunar regolith simulants. Roller mass is another critical parameter influencing compaction depth, uniformity, and effectiveness.

In recent investigations, including those by Scott et al. (2023) and Agarwal et al. (2024, 2026a, 2026b), lunar highlands regolith simulants have been widely employed due to the extremely limited availability of actual lunar samples. Owing to the unobtainability of actual lunar highland regolith samples, simulants are routinely adopted for experimental research (Slabic et al., 2024; Toklu and Akpinar, 2022). The present study utilises LHS-1E, an engineering-grade lunar highlands simulant composed of 75% anorthosite and 25% basalt, developed to replicate the mineralogical and particle size distribution characteristics of lunar highland regolith (Space Resource Technologies, 2021). Previous work by Agarwal et al. (2023) demonstrated that LHS-1E exhibits geotechnical properties representative of actual lunar regolith, supporting its suitability for experimental investigations.

The present study focuses on selected optimal and comparative operating conditions to provide a more comprehensive evaluation of compaction behaviour. For the 2.92 kg roller mass, operating conditions of 2 km/h at 40 Hz and 4 km/h at 30 Hz were investigated, while for the 4.45 kg roller mass, conditions of 2 km/h at 40 Hz and 6 km/h at 40 Hz were examined. This work systematically evaluates multiple key performance indicators—including surface settlement, in situ density, cone tip resistance, pressure, and acceleration across different test lanes prepared under identical initial conditions. This approach enables a robust assessment of the coupled effects of roller mass, vibration frequency, and operating speed on the compaction behaviour of lunar highlands regolith simulants, thereby addressing a critical gap in current knowledge and providing essential insights for the design and implementation of mechanised compaction strategies in lunar infrastructure development.

3. METHODOLOGY

Figure 1 shows two bins, each measuring 750 mm in width and 1060 mm in length, which were used for testing. In this study, the lunar highland regolith simulant (LHS-1E) was placed to a depth of 380 mm, and was intentionally placed in a loose state to replicate lunar surface conditions and to evaluate the extent to which a lunar vibrating drum roller (LVDR-1) can improve the density of LHS-1E. The LVDR-1 model was mobilised along the test lane using a chain-driven carriage system powered by a variable-speed electric motor.

To achieve identical densities of the LHS-1E simulant in each bin, a target bulk density of 1500 kg/m^3 was adopted for the LHS-1E simulant. This density represents a loose regolith simulant condition and was selected as it can be reproducibly achieved under terrestrial laboratory conditions, which closely represent the density of near-surface lunar regolith. The adopted density lies within the typical range of lunar regolith densities 870 kg/m³ –1930 kg/m³ reported from Apollo mission samples and documented in the Lunar Sourcebook (Heiken et al. 1991). Due to the inability to replicate the lunar environment (vacuum, presence of agglutinates, reduced gravity) in laboratory conditions, the lower-bound densities reported by Heiken et al. (1991) could not be achieved. To define the attainable density range, minimum and maximum densities of 1450 kg/m³ and 2000 kg/m³, respectively, were determined in accordance with AS 1289.5.5.1 (Standards Australia, 1998), as reported by Agarwal et al. (2023). Based on the minimum and maximum densities reported by Agarwal et al. (2023) and using Equation 1, the initial placement density corresponds to a relative density (RD) of 12%.

$$RD\ (\%) = \frac{\rho_{max}}{\rho} \times \frac{\rho - \rho_{min}}{\rho_{max} - \rho_{min}} \times 100 \quad (1)$$

where: ρ, ρ_{min} and ρ_{max} are the in situ, minimum and maximum densities, respectively. As a result, approximately 404 kg of simulant was placed in each bin.

Figure 1. Test setup.

To achieve a homogeneous target density in each bin, the simulant was weighed and carefully placed into each bin using 5-litre buckets. The LHS-1E was pluviated through a 2.36 mm sieve, with the fall height controlled to not exceed 200 mm, as shown in Figure 2. To further enhance uniformity, the simulant was placed in 50 mm thick layers and screeded against timber formwork placed around the perimeter of the bins to achieve consistent placement. Although this process was time-consuming, the results presented later demonstrate excellent agreement with the target density.

The placement process was further complicated by dust generation. Given the desiccated nature of the simulant, its high fines content, and associated health and safety considerations, appropriate personal protective equipment, including safety glasses, masks, coveralls, and gloves, was worn during placement of the LHS-1E simulant.

Figure 2. Pluviation of LHS-1E simulant during placement.

The LVDR-1 scale model used in the experiments is shown in Figure 3. Testing was conducted using two distinct drum roller masses, 2.92 kg and 4.45 kg, with each configuration tested independently. Upon completion of testing with the 2.92 kg mass, the soil bins were fully emptied and replaced at the same targeted bulk density prior to testing with the 4.45 kg mass. This approach ensured that the influence of roller mass on compaction behaviour could be isolated and evaluated under comparable initial conditions. To achieve a mass of 4.45 kg, four rectangular steel blocks mounted two on each side of the motor were affixed to the frame using screws without direct contact with the drum to increase the total roller mass by approximately 50%, as shown in Figure 3b. While this method enabled controlled variation of drum mass, it represents a limitation of the scale model, as the added mass was positioned externally rather than incorporated as eccentric mass within the drum itself, as typically occurs with terrestrial vibrating drum rollers.

The scale model incorporates a drum with a width of 165 mm and a diameter of 100 mm, representing a scaled aspect ratio comparable to full-sized terrestrial rollers. Vibratory frequency was generated using an externally mounted electric motor fitted with an eccentric mass and mounted on the drum axle (Figure 3c). The rotational speed of the motor was adjusted to control the vibration frequency with higher fidelity, allowing consistent and repeatable loading conditions across tests.

To verify the applied vibration frequencies, Fast Fourier Transform (FFT) analysis was performed on data collected from earth pressure cells (EPCs) buried in each lane. This

analysis confirmed that the target frequencies were achieved. It is acknowledged that, while these experiments provide valuable insight into compaction behaviour under controlled laboratory conditions, the response of actual lunar regolith may differ due to the Moon's reduced gravity, vacuum environment, and electrostatic effects.

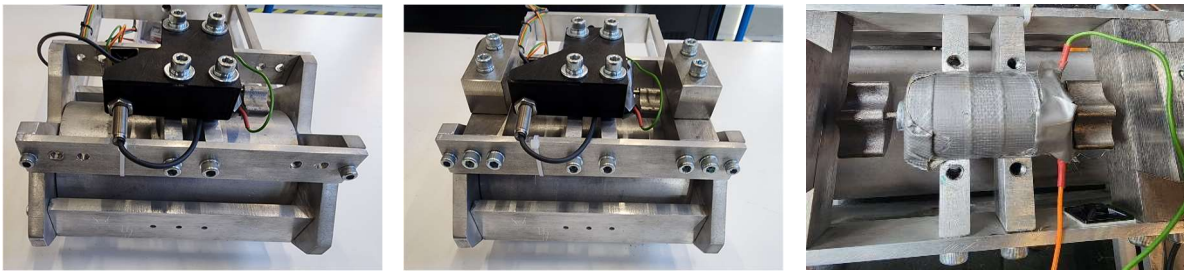

(a) **(b)** **(c)**

Figure 3. LVDR-1 scale model: (a) 2.92 kg version; (b) 4.45 kg version; (c) Electric vibration motor.

For the 2.92 kg drum roller mass, two configurations were selected: 2 km/h at 40 Hz and 4 km/h at 30 Hz. The first configuration was chosen based on promising compaction performance reported by Agarwal et al. (2026b), while the latter configuration is included to allow direct comparison with initial experimental testing conducted at this speed by Agarwal et al. (2024, 2026a). For the 4.45 kg drum roller mass, tests were conducted at 2 km/h and 6 km/h, both at a vibration frequency of 40 Hz. The first configuration was selected to allow direct comparison with the lighter mass, and the latter configuration was chosen based on its peak pressure performance reported by Agarwal et al. (2026b). This study aims to directly compare the compaction performance of the most promising combination of roller mass, speed and frequency using buried EPCs and accelerometers, and pre- and post-compaction in situ testing.

Figure 4 represents a schematic setup of the test bins for the 2.92 kg drum roller mass, showing the lane configuration and rolling direction for the LVDR-1 model. Two large, instrumented soil bins were positioned beneath the elliptical track, however, they can be translated perpendicular to the roller's direction of travel to allow for lane changes, and better access for bin filling and testing. This arrangement enabled the formation of three separate lanes (Lanes 1–3 as shown in Figure 4a) without altering the position of either the scale model roller or the track, thereby ensuring consistent operating conditions across all tests and allowing for systematic, repeatable comparisons between lanes.

For the 2.92 kg roller mass, Lane 1 was compacted at a speed of 2 km/h with a vibration frequency of 40 Hz, while Lane 3 was compacted at 4 km/h and 30 Hz, as indicated in Figure 4a. Lane 2 remained unrolled and served as a separation zone between the two compacted lanes. A spacing of 210 mm, corresponding to the width of Lane 2, was maintained between Lanes 1 and 3 to minimise interaction effects and ensure independent compaction responses. Figure 4a also indicates the locations of the various tests conducted within each lane to evaluate their influence on compaction efficiency and uniformity in the LHS-1E simulant.

Figure 4b illustrates the placement of the EPCs within the simulant. Six EPCs were installed in total, with three embedded in each of Lanes 1 and 3 at depths of 50, 100, and 150 mm, respectively. The EPCs were spaced laterally at intervals of 100 mm and vertically at 50 mm. To reduce boundary effects, the distance from the bin wall to the centerline of each compacted lane was maintained at 187.5 mm. The overall bin setup was designed to mitigate EPC shadowing beneath the centreline of each lane during operation (Dave and Dasaka 2011).

An identical bin setup was adopted for the heavier 4.45 kg roller mass, with only the operational parameters varied. In this case, Lane 1 was operated at 2 km/h and 40 Hz, while Lane 3 was compacted at 6 km/h and 40 Hz, with Lane 2 again left unrolled. For both roller masses, the rolling direction was maintained from Bin A to Bin B, as shown in Figure 4.

The compaction testing was conducted sequentially in both lanes, following a consistent pattern to minimise potential interaction between lanes. Initially, Lane 1 was compacted for the first five passes, followed by five passes in Lane 3. After completion of these initial passes, density testing was conducted in each lane, as well as in Lane 2 (no rolling). Subsequently, the remaining 15 passes (Passes 6–20) were completed in Lanes 1 and 3, respectively, followed by final density measurements in each lane, as well as in Lane 2 (i.e. no rolling). The entire testing was completed over a two-day period.

To assess the potential influence of natural settlement of the loose simulant during the testing period, surface settlement measurements were recorded in each rolling lane after every pass and again prior to the continuation of testing on the second day. It was observed that the simulant remained stable throughout the experiment, with no measurable settlement occurring overnight between the two testing days.

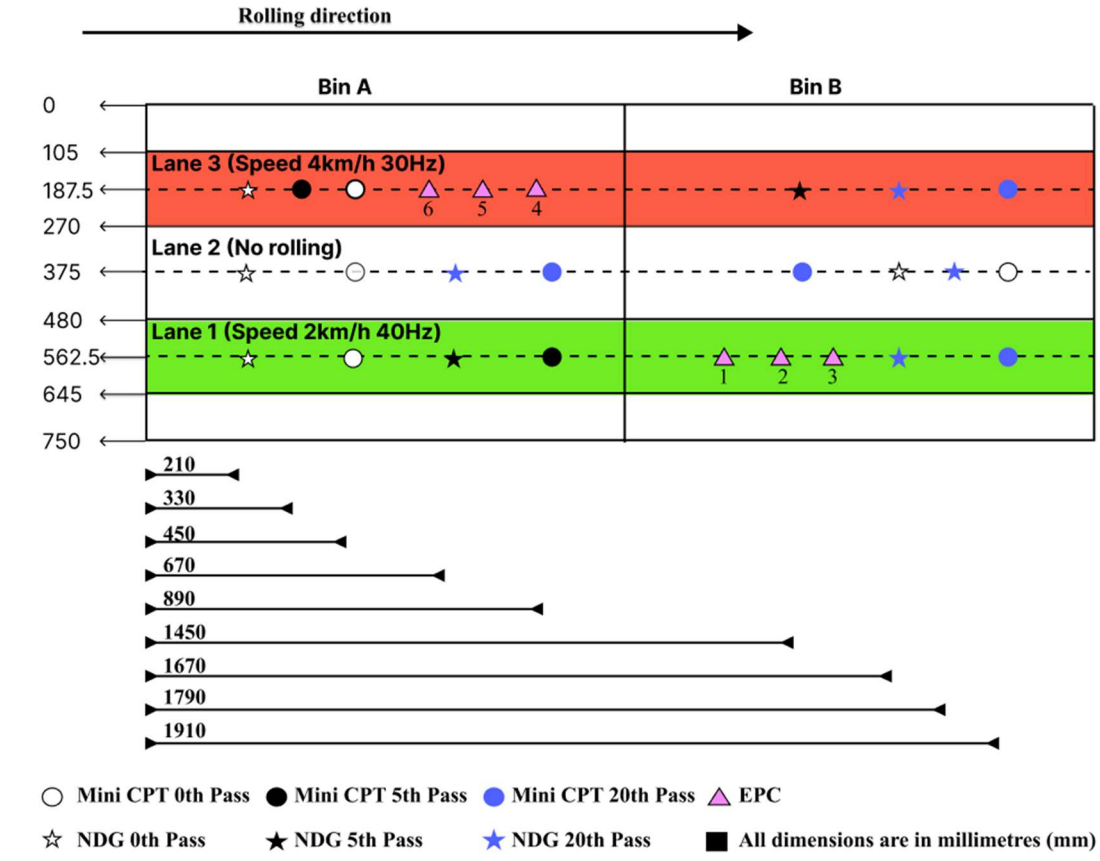

(a)

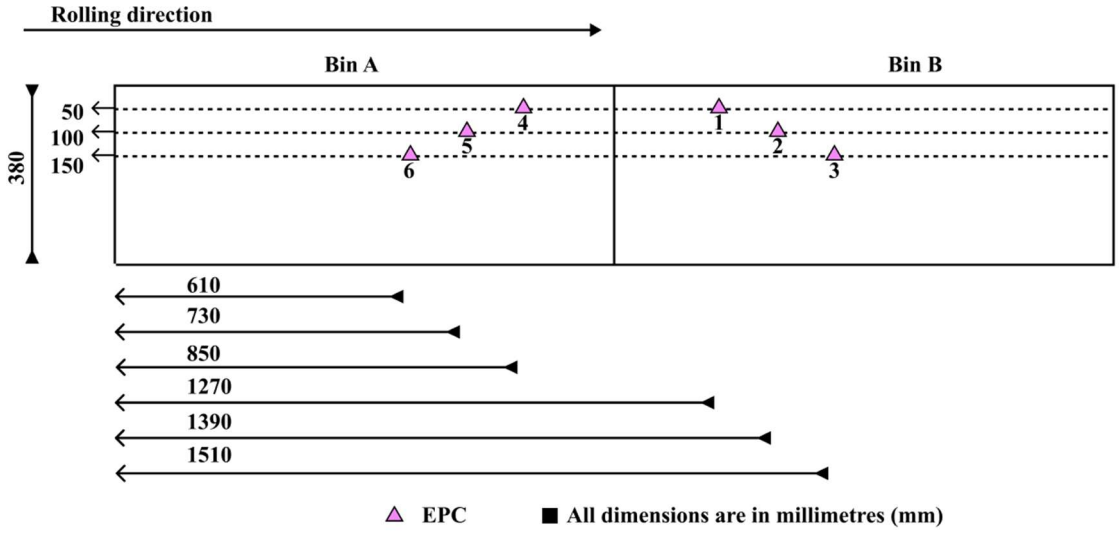

(b)

Figure 2. Schematic of the 2.92 kg bin setup: (a) Plan view showing testing locations; (b) Elevation view indicating embedment depths.

As illustrated in Figure 5a, the bespoke EPCs used in this study have a diameter of 19 mm and are equipped with integrated tri-axial accelerometers as shown in Figure 5bFigure 3. Earth pressure cell: (a) Plan view; (b) Internal 3-axis accelerometers.. While conventional EPCs with larger diameters are widely employed in geotechnical engineering for terrestrial in situ earth pressure measurements (e.g. Rinehart and Mooney, 2009, Scott et al., 2019), the reduced dimensions of the bespoke sensors enabled detailed monitoring within the scaled,

confined test environment. Each EPC–accelerometer assembly was connected to a custom-built data acquisition system interfaced with a dedicated LabVIEW program, providing simultaneous measurement of contact pressures and ground accelerations during compaction. Prior to testing, all EPCs were zeroed to remove the influence of overburden pressure, ensuring that only roller-induced stresses were recorded. For each depth, peak pressure values were obtained by averaging measurements from 20 roller passes. To ensure accurate capture of peak pressure responses and high-frequency vibration effects, a sampling frequency of 7500 Hz was adopted.

(a) **(b)**

Figure 3. Earth pressure cell: (a) Plan view; (b) Internal 3-axis accelerometers.

Surface settlement measurements were systematically performed to quantify vertical displacement, using the elliptical track as a frame of reference. A standard tape measure was used in conjunction with fixed reference bolts as can be observed in Figure 1, which were repeatable measurement points throughout the testing phase. For each lane, a total of 20 passes were completed, with 10 surface settlement measurements obtained after each pass. The mean of these readings was calculated to represent the surface settlement corresponding to each test lane. For each lane, initial measurements were obtained prior to any compaction passes and treated as the baseline for that specific lane, allowing subsequent surface deformation to be assessed relative to its own starting condition.

In situ density measurements were obtained using a nuclear density gauge HS-5001SD (Humboldt Mfg. Co., 2026) in accordance with the relevant manual (Humboldt Mfg. Co., 2020) and Australian Standard (Standards Australia, 2007). The nuclear density gauge (NDG) determines in situ density using a gamma radiation source (caesium-137), and is a technique that is widely adopted for field density testing of compacted soils due to its rapid and (relatively) non-destructive measurement capability (Bretreger, 2015). Measurements were conducted both prior to compaction and after 5 and 20 roller passes of the LVDR-1 model in each lane for both roller masses. Owing to the limited dimensions of the test bins, three measurement locations were assessed per lane at each testing stage. The locations of these measurements are illustrated in Figure 4a. The surface of the simulant was screeded slightly to have optimal contact between the instrument and the surface. Density readings were initially taken at a depth of 50 mm, followed by measurements at 25 mm depth increments down to a maximum depth of 300 mm. At each depth, three measurements were recorded and averaged to represent the in situ density. If the variation between measurements exceeded 0.5%, an additional test was conducted at that depth.

Mini cone penetration tests (mini-CPTs) were performed using a Geomil digital cone penetrometer with a 25 mm shaft diameter, 500 mm^2 cone cross-sectional area, and 60° apex angle (Geomil, 2026). The mini-CPT uses a cone at the end of a rod, which was manually pushed into the simulant perpendicular to the surface at a controlled penetration rate of

approximately 20 mm/s, in accordance with the standard testing procedure (Standards Australia 1999). This controlled rate ensured accurate measurement of cone tip resistance and minimised errors due to variations in penetration velocity. Cone resistance was recorded at 10 mm depth intervals, while penetration depth was monitored using a synchronised depth encoder. The cone penetration resistance was measured prior to compaction and after 5 and 20 passes in each lane. The mini-CPT measurements were directly compared with NDG-derived densities to verify the consistency and robustness of the inferred density profiles, thereby strengthening the interpretation of compaction behaviour in the lunar highland regolith simulant.

The above-mentioned methodology was applied consistently for both roller masses, 2.92 kg and 4.45 kg of the LVDR-1 model, across all measurements, including EPC recording, surface settlement assessment, NDG measurement and cone penetration resistance testing, thereby ensuring direct comparability of the results.

4. RESULTS AND DISCUSSION

Figure 6 illustrates the results of surface settlement with increasing roller passes for the LVDR-1 scale model, providing a quantitative assessment of compaction behaviour under varying roller mass, operating speed, and vibration frequency. A total of 20 roller passes was applied in each compaction lane. Figure 6a corresponds to a drum roller mass of 2.92 kg, whereas Figure 6b corresponds to the drum roller mass of 4.45 kg. For the 2.92 kg roller mass, tests were conducted under two operating conditions: (i) Lane 1 at a speed of 2 km/h and a vibration frequency of 40 Hz, and (ii) Lane 3 at a speed of 4 km/h and a frequency of 30 Hz. For the 4.45 kg roller mass, compaction was performed at (i) 2 km/h at 40 Hz in Lane 1, and (ii) 6 km/h at 40 Hz in Lane 3. As described in Section 3, after completing tests with the 2.92 kg roller mass, the soil bins were reset to the same target bulk density prior to testing with the 4.45 kg roller mass, ensuring that the influence of roller mass on compaction behaviour was evaluated under comparable initial conditions.

In both masses of LVDR-1, the first roller pass produced the largest settlement, consistent with previous findings (Agarwal et al., 2024, 2026a, 2026b), reflecting the very loose initial placement condition of the lunar regolith highland simulant. Figures 6a and 6b further show that the majority of surface settlement occurred within the first 10 passes, regardless of roller mass or operating conditions. Beyond this stage, the subsequent passes resulted in only marginal additional settlement, indicating a progressive stabilisation of surface deformation. This trend confirms that the rate of settlement decreases with increasing number of passes, which is consistent with expected compaction behaviour.

After 20 passes, the surface settlement for LVDR-1 with a roller mass of 2.92 kg was recorded as 28 mm and 16 mm for operating conditions of 2 km/h at 40 Hz and 4 km/h at 30 Hz, respectively. In contrast, the LVDR-1 with a roller mass of 4.45 kg induced higher settlements of 39 mm and 34 mm for operating conditions of 2 km/h at 40 Hz and 6 km/h at 40 Hz, respectively. These results demonstrate that a heavier roller mass, higher vibration frequency, and lower operating speed significantly enhance surface settlement in lunar highlands regolith simulant. Among the tested conditions, the configuration with a roller mass of 4.45 kg operating at 2 km/h and 40 Hz induced the largest surface settlement.

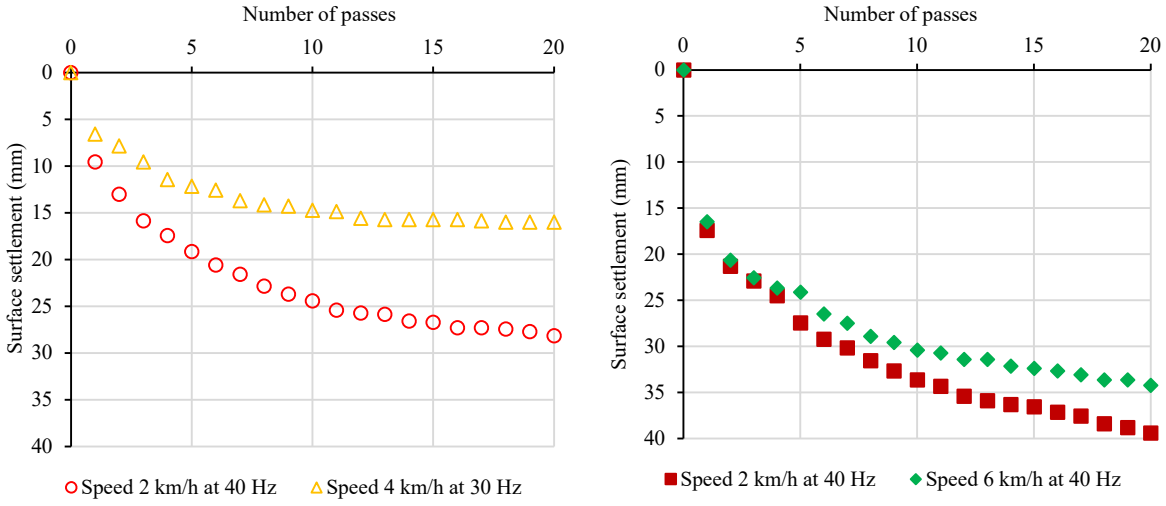

(a) **(b)**

Figure 4. Average surface settlement versus number of passes: (a) 2.92 kg; (b) 4.45 kg.

Figure 7 illustrates the in situ density with depth below the ground surface for varying numbers of roller passes. Figures 7a and 7b correspond to the LVDR-1 model with a drum mass of 2.92 kg operating at speeds of 2 km/h and 4 km/h with vibration frequencies of 40 Hz and 30 Hz, respectively. Figures 7c and 7d represent the mass of 4.45 kg of LVDR-1 model operating at speeds of 2 km/h and 6 km/h, both at a frequency of 40 Hz.

Target placement density was set at 1500 kg/m³ for both roller masses; however, the achieved initial in situ densities after soil bin preparation exhibited slight variations. For the 2.92 kg roller mass, an initial density of 1550 kg/m³ was obtained, corresponding to a relative density of approximately 23%. For the 4.45 kg roller mass, the initial density was 1514 kg/m³, corresponding to a relative density of approximately 15%. These densities represent the average density of each bin throughout its depth and across the entire volume. The observed minor deviations from the target density may be attributed to slight variations in particle packing and modest inconsistencies while filling and levelling the bins during preparation. Despite these minor variations, the uniform density profiles with depth in both cases confirmed comparable initial conditions. These achieved densities and the corresponding relative densities were therefore adopted as the baseline for subsequent compaction roller passes.

Figures 7a–7d show that compaction using the LVDR-1 results in a measurable increase in density after the first five passes for both roller masses. However, for the 2.92 kg roller mass, density improvement becomes marginal beyond 20 passes. In contrast, the 4.45 kg roller mass continues to exhibit progressive density enhancement, demonstrating a greater capacity for densification under otherwise identical operating conditions. This behaviour is consistent with the surface settlement results, which show limited additional settlement beyond five passes for the 2.92 kg roller mass, whereas substantial settlement persists for the 4.45 kg roller mass.

Across both roller masses, the operating condition of 2 km/h at 40 Hz consistently produced the highest degree of density improvement, indicating that lower operating speed,

combined with higher vibration frequency, provides more effective energy transfer to the lunar simulants, thereby enhancing densification of the simulant.

At a depth of 75 mm, the recorded densities after 20 passes were 1734, 1676, 1727, and 1672 kg/m³ for Figures 7a, 7b, 7c, and 7d, respectively. These values correspond to relative densities of 60%, 49%, 58%, and 48%, respectively. At a depth of 300 mm, the corresponding densities were 1650, 1585, 1621, and 1571 kg/m³, yielding relative densities of 44%, 31%, 38%, and 28%, respectively. These results demonstrate a clear reduction in densification efficiency with increasing depth, highlighting damping of vibratory energy propagation within the simulant.

Measurements were also conducted in the no-rolling (i.e. middle) lane to evaluate the lateral influence of LVDR-1 on adjacent lanes, and the results are presented in Figures 7e and 7f. It can be observed from that compaction effects extend beyond the directly loaded lane, as one might expect, with the heavier roller mass exerting a greater influence compared to the lighter configuration. This lateral densification effect provides evidence of cross-lane vibratory energy transmission and demonstrates that roller mass governs not only vertical compaction efficiency but also the spatial extent of soil improvement. This is consistent with observations of terrestrial compaction.

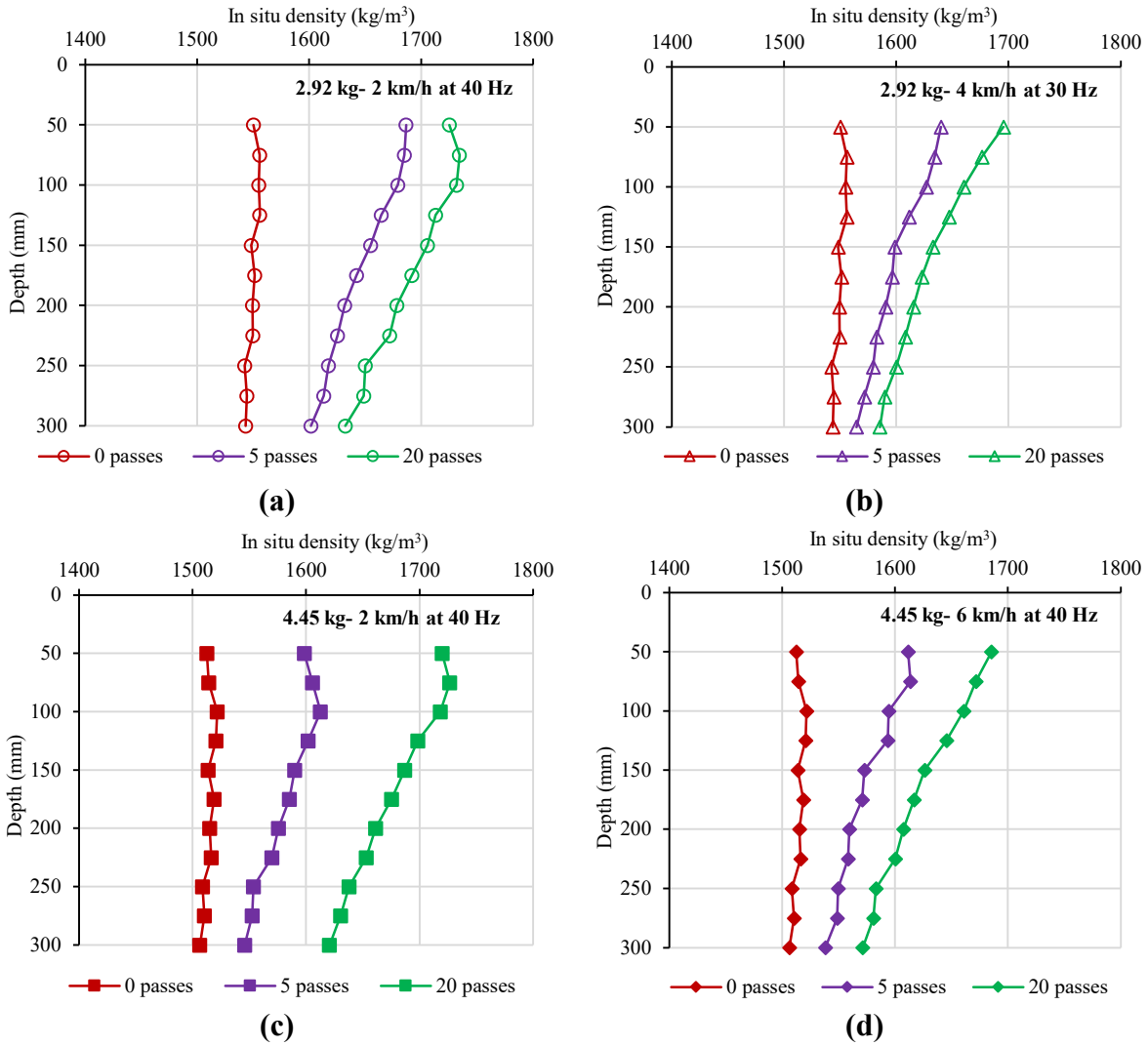

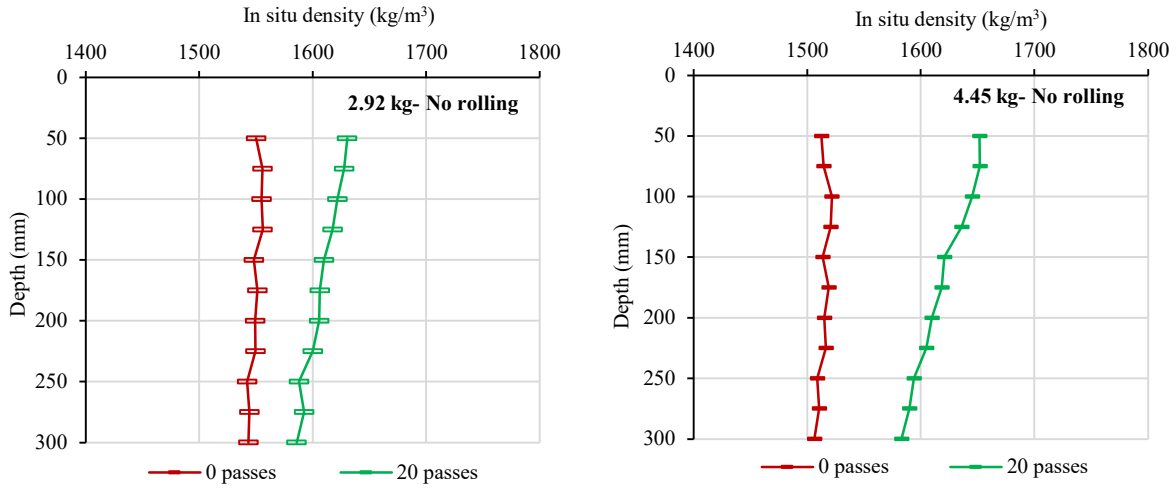

(e) **(f)**

Figure 5. Measured in situ density of lunar highland regolith simulant using the LVDR-1, results are shown for 0, 5, and 20 roller passes for: (a) 2.92 kg at 2 km/h and 40 Hz; (b) 2.92 kg at 4 km/h and 30 Hz; (c) 4.45 kg at 2 km/h and 40 Hz; (d) 4.45 kg at 6 km/h and 40 Hz. Reference profiles corresponding to unrolled lanes are presented for (e) 2.92 kg and (f) 4.45 kg.

Figure 8 shows the results of the relative density (RD) difference with depth for the operating condition of 2 km/h at 40 Hz for both roller masses. This operating condition was selected because the results shown above demonstrated that a lower speed, combined with a higher vibration frequency, yields the most effective densification response. The relative density difference represents the change between the pre-compaction state (0 passes) and the post-compaction state after 20 passes. At a depth of 75 mm, the RD difference is 35% and 43% for the 2.92 kg and 4.45 kg roller masses, respectively, while at a depth of 300 mm the corresponding values decrease to 19% and 25%. It is clearly evident that the heavier roller mass produces a consistently higher relative density than the lighter roller mass across all depths, indicating more effective transmission of vibratory energy into the subsurface. The superior performance of the heavier roller mass is further corroborated by the surface settlement measurements, which show greater settlement under the 4.45 kg roller mass. Overall, the results confirm that roller mass plays a dominant role in governing subsurface densification under low-speed, high-frequency vibration, and that increased inertial loading is critical for achieving deeper and more uniform compaction of lunar highland regolith simulant.

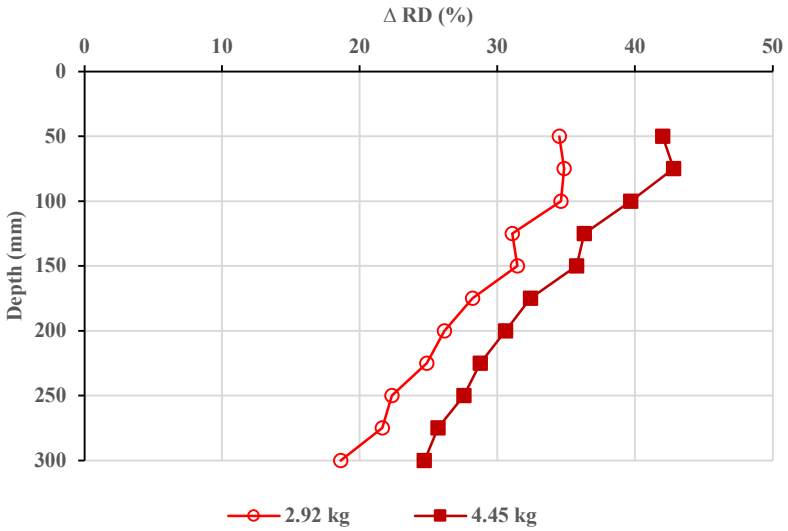

Figure 6. Change in relative density between pre-compaction (0 passes) and post-compaction (20 passes) for the operating condition of 2 km/h at 40 Hz: (a) 2.92 kg; (b) 4.45 kg.

Figure 9 illustrates cone tip resistance profiles with depth corresponding to different numbers of roller passes. Figures 9a and 9b correspond to the LVDR-1 with a drum mass of 2.92 kg operating at speeds of 2 km/h and 4 km/h with vibration frequencies of 40 Hz and 30 Hz, respectively. Figures 9c and 9d represent the LVDR-1 with a roller mass of 4.45 kg operating at speeds of 2 km/h and 6 km/h, both at a frequency of 40 Hz.

The pre-compaction condition (Pass 0) for both roller masses, shown in Figure 9, exhibits a monotonic increase in cone tip resistance with depth, which is consistent with the expected cone penetration response in a soil mass of approximately uniform density, where resistance is governed primarily by increasing overburden stress rather than compaction-induced densification (Lunne et al., 2002; Robertson, 2009).

For both roller masses, cone tip resistance increases significantly from the baseline at shallow depths after 5 and 20 passes, but diminishes progressively with depth, indicating attenuation of vibratory compaction effects with depth. These trends are consistent with the density results presented in Figure 7, which also demonstrate increasing densification with roller passes. Higher cone tip resistance, therefore, reflects greater local densification of the simulant.

For the 2.92 kg roller mass, the penetration resistance profiles indicate that lower operating speed combined with higher vibration frequency produces the most pronounced increase in cone tip resistance throughout the soil profile. In contrast, the lower vibration frequency exhibits negligible influence beyond approximately 200 mm depth, indicating limited penetration of vibratory energy into the simulant, as shown in Figures 9a and 9b. This behaviour is consistent with the in situ density results presented in Figures 7a and 7b, where the operating condition of 2 km/h at 40 Hz also produced the greatest density enhancement.

In the case of the 4.45 kg roller mass, cone penetration resistance values are consistently higher at lower operating speeds, indicating greater densification under slower roller velocity. At the same vibration frequency of 40 Hz, both operating speeds exhibit

increased penetration resistance extending to greater depths, highlighting the dominant role of vibration frequency in controlling subsurface compaction. A similar trend is observed for density shown in Figures 7c and 7d, where the heavier roller mass generates greater density improvement throughout the depth profile.

Figures 9e and 9f correspond to the no-rolling lane, where no direct compaction was applied. Nevertheless, an increase in cone penetration resistance is observed in these lanes, indicating lateral transmission of vibratory energy from the adjacent compacted lanes. This behaviour is also reflected in the density measurements presented in Figures 7e and 7f, confirming that vibratory energy propagates laterally beyond the directly loaded lane and contributes to partial densification of the surrounding simulant. This confirms that the influence of vibratory compaction is not confined to the intended testing lane, but affects a broader area.

Post-compaction assessment suggests that the adopted lane configuration does not adequately isolate the vibration compaction effects, with the spacing between Lanes 1 and 3. For future scale model studies involving VSDR, increased edge distances and greater separation between adjacent lanes are therefore recommended to minimise boundary effects and ensure more representative density measurements.

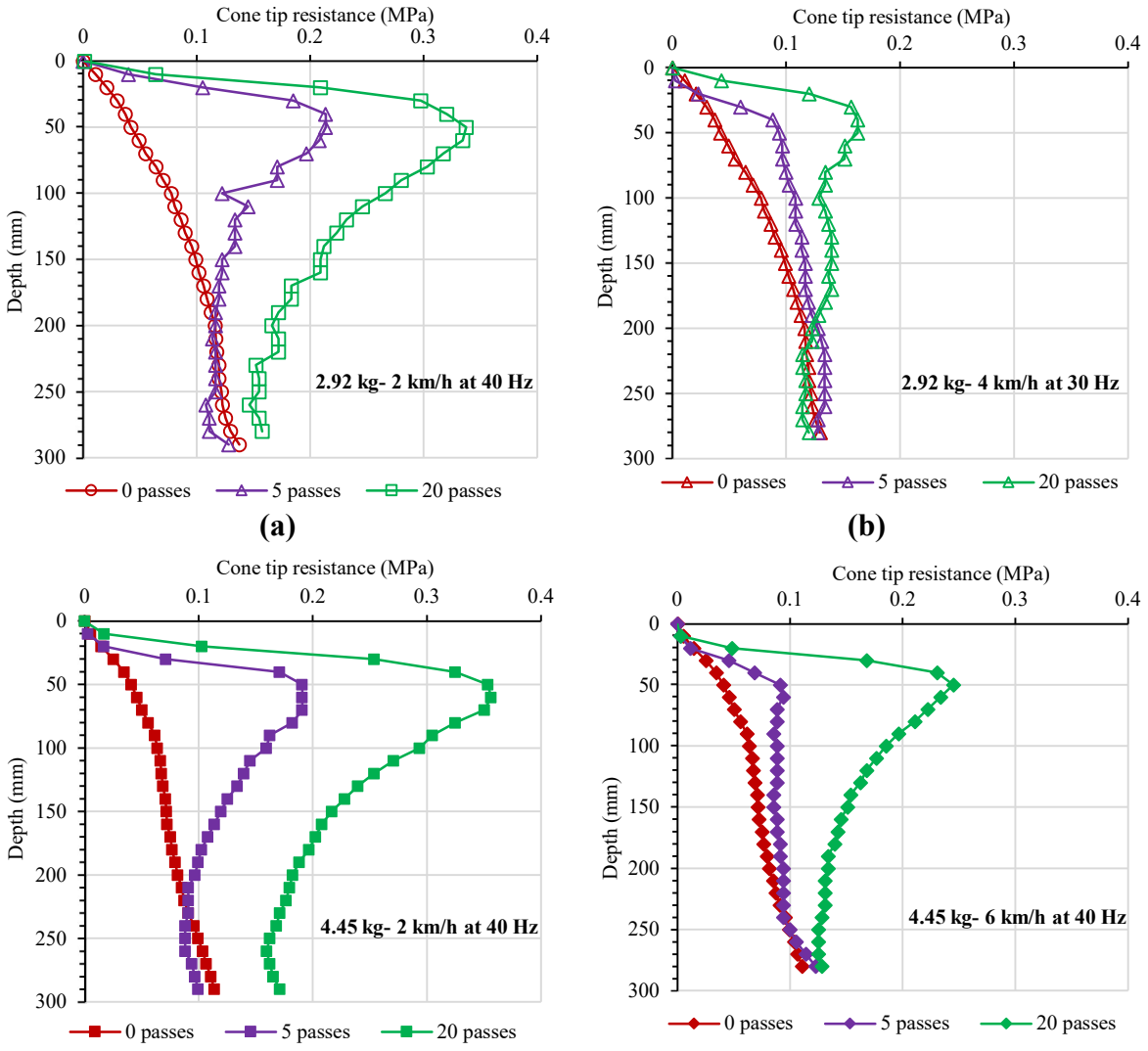

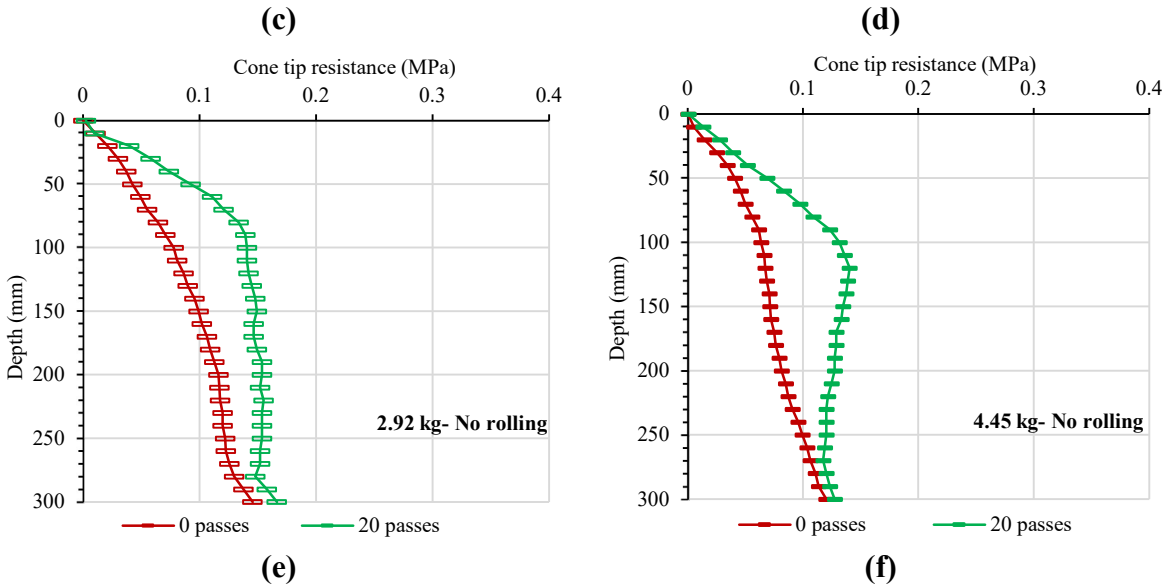

458 **Figure 7. Resistance vs depth results are shown for 0, 5, and 20 roller passes for: (a) 2.92**
459 **kg at 2 km/h and 40 Hz; (b) 2.92 kg at 4 km/h and 30 Hz; (c) 4.45 kg at 2 km/h and 40**
460 **Hz; (d) 4.45 kg at 6 km/h and 40 Hz. Reference profiles corresponding to unrolled lanes**
461 **are presented for (e) 2.92 kg; (f) 4.45 kg.**
462
463 Figure 10 displays the dynamic pressure response of the simulant during the 20th pass
464 of LVDR-1, with a drum mass of 2.92 kg operating at 2 km/h and 40 Hz in Lane 1. Pressure
465 measurements obtained from EPCs 1, 2, and 3 buried at depths of 50 mm, 100 mm, and
466 150 mm, respectively, indicate that peak stresses are highest near the surface and decrease
467 with depth, which is consistent with the findings reported by Rinehart and Mooney (2009).
468 The time interval at which each EPC records the peak pressure is dependent on the EPC
469 placement location, as shown previously in Figure 4. The pressure response shown in
470 Figure 10 appears 'noisy' due to the oscillations of the roller motor over the 20-second
471 measurement period and these fluctuations arise from the combined effects of the periodic
472 vibration generated by the roller's oscillating motor and transient soil–roller interaction
473 during drum contact and lift-off (Richart et al., 1970; Mooney and Rinehart, 2009).
474

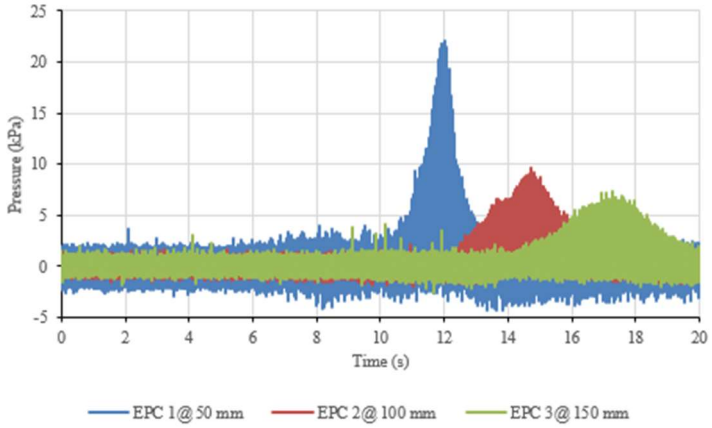

475
476 **Figure 8. Pressure response during the 20th pass of the LVDR-1 (2.92 kg, 2 km/h at**
477 **40 Hz)**

Figure 11 presents the measured peak pressures plotted against depth below the ground surface for both roller masses. For each lane, peak pressure data from all three EPCs, which were placed at depths of 50 mm, 100 mm and 150mm, were averaged across all 20 passes at each depth. For the 2.92 kg roller mass (Figure 11a), the averaged peak pressure at 50 mm depth was 18 kPa for the operating condition of 2 km/h at 40 Hz and 10 kPa for 4 km/h at 30 Hz in Lanes 1 and 3, respectively. At 150 mm depth, the corresponding values decreased to 7 kPa and 4 kPa, respectively. These results demonstrate that lower speed combined with higher vibration frequency generates higher peak pressures throughout the lunar simulant profile.

For the 4.45 kg roller mass (Figure 11b), the averaged peak pressure at 50 mm depth was 24 kPa for 2 km/h at 40 Hz and 17 kPa for 6 km/h at 40 Hz, while at 150 mm depth the values reduced to 10 kPa and 7 kPa, respectively. Under constant frequency, the lower operating speed produced consistently higher peak pressures at all depths.

The highest stress levels were observed at shallow depth (50 mm), with progressively lower magnitudes recorded at depths of 100 mm and 150 mm. This indicates the reduction of vibratory stress transmission with depth and is consistent with established findings on vibratory compaction in granular soils (Richart et al., 1970; Massarsch and Fellenius, 2005). A comparison between Figures 11a and 11b indicates that the heavier roller mass operating at a lower speed and higher frequency produces greater peak pressures across the depth profile than the lighter roller mass. This trend is consistent with the surface settlement and in situ density results, confirming the dominant role of heavier roller mass, lower speed and higher frequency in controlling subsurface stress transmission and compaction effectiveness.

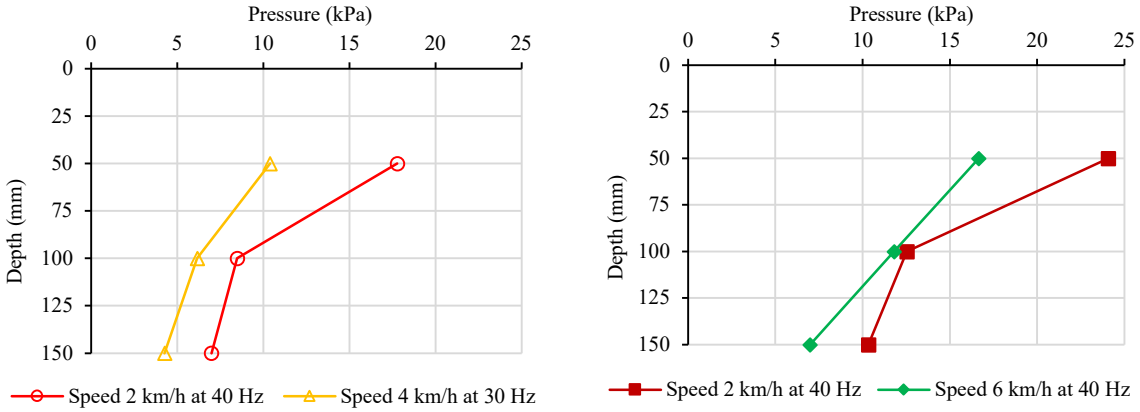

(a) **(b)**

Figure 9. Peak pressure vs depth, averaged over all 20 passes: (a) 2.92 kg; (b) 4.45 kg.

Figure 12 presents the vertical acceleration response over a one-second window, spanning 0.5 seconds on either side of the time corresponding to the peak pressure. The measurements were obtained at a constant depth of 50 mm, while roller mass, operating speed, and vibration frequency were varied in Figure 12.

For the 2.92 kg roller mass, the vertical acceleration amplitude in Figure 12a is approximately three times greater than that in Figure 12b. This difference is attributed to the combination of lower speed 2 km/h and higher frequency 40 Hz in Figure 12a, compared with

higher speed 4 km/h and lower frequency 30 Hz in Figure 12b. These results demonstrate that, for the lighter roller mass, lower speed coupled with higher frequency generates a significantly stronger dynamic response and greater subsurface acceleration.

For the 4.45 kg roller mass, the vertical acceleration amplitude in Figure 12c is approximately twice that observed in Figure 12d. Since the frequency is identical i.e., 40 Hz in both cases, this difference is primarily governed by operating speed, with the lower speed of 2 km/h producing a substantially higher in-ground acceleration response than the higher speed of 6 km/h. The similar acceleration peak responses observed in Figures 12a and 12c, obtained under identical speed and vibration frequency with only the roller mass varied, indicate that an increase in roller mass does not necessarily result in higher measured vertical accelerations.

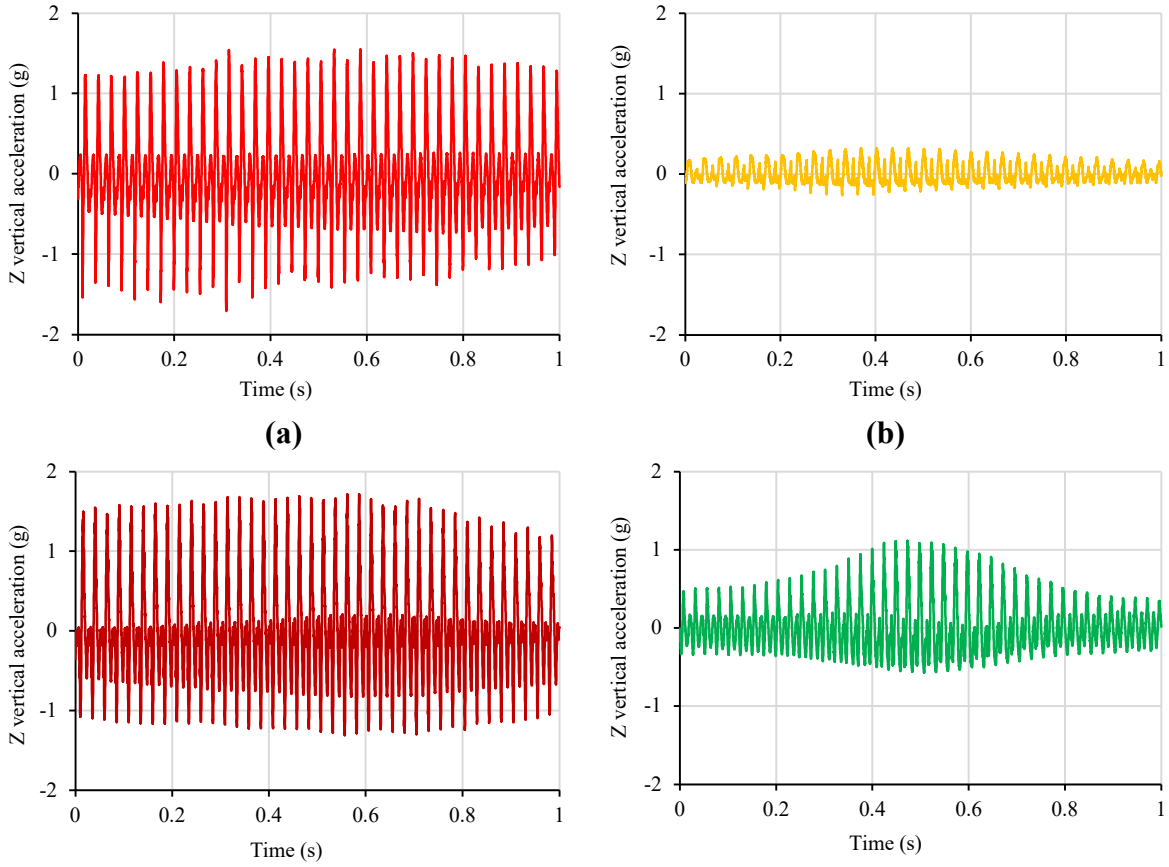

Figure 10. Vertical acceleration responses beneath the roller over a 1-second window at 50 mm depth: (a) 2.92 kg at 2 km/h and 40 Hz; (b) 2.92 kg at 4 km/h and 30 Hz; (c) 4.45 kg at 2 km/h and 40 Hz; (d) 4.45 kg at 6 km/h and 40 Hz.

CONCLUSION

The present study provides a comprehensive assessment of the effects of roller mass, operating speed, and vibration frequency on the dynamic compaction of lunar highlands regolith simulants. The experimental results demonstrate that lower roller speeds combined with higher vibration frequencies consistently produce the most pronounced densification

throughout the lunar simulant profile, as evidenced by surface settlement measurements, in situ density tests, cone penetration tests and vertical stress measurements. Peak stress and cone tip resistance measurements revealed the highest values at shallow depths, with a progressive attenuation of vibratory stress transmission with depth, consistent with established soil compaction and vibratory stress propagation principles

Comparison between roller masses highlights that, although a heavier roller mass contributes to increased compactive resistance, vibration frequency has a greater influence on the depth and magnitude of simulant densification than mass alone. The surface settlement data further strengthens these observations, demonstrating that the most efficient densification response occurred with the 4.45 kg roller operating at 2 km/h and 40 Hz.

Overall, the results emphasise that optimal compaction is achieved through the careful selection of operating speed and vibration frequency, rather than by increasing roller mass alone. The combined interpretation of surface settlement, density measurements, and cone penetration resistance results indicate that higher vibration frequencies enhance the transmission of dynamic stresses through the simulant, enabling deeper zones of influence and improved densification efficiency. These findings provide mechanistic insights into vibratory energy propagation, stress attenuation, and densification behaviour that are essential for extraterrestrial lunar highlands regolith improvement strategies.

It is also essential to acknowledge that the compaction behaviour of lunar regolith may differ significantly under the Moon's unique environmental conditions, including reduced gravity, vacuum, and exposure to electrostatically charged particles. These environmental factors may influence particle rearrangement, stress transmission, and vibratory energy dissipation within the regolith, potentially altering compaction performance compared with terrestrial conditions. Importantly, this study provides novel experimental evidence on the parametric interplay within the LVDR-1 model between roller mass, vibration frequency, and operating speed in lunar highland regolith simulants, thereby advancing current understanding of compaction mechanism and contributing to the development of engineering methodologies tailored for extraterrestrial infrastructure applications.

Looking forward, modifications to drum geometry and eccentric mass configuration may further enhance vibratory energy transfer and improve compaction performance. Such investigations will enable the identification of the most effective combination of roller mass, aspect ratio, and intelligent compaction approaches for lunar surface applications, further advancing the engineering of extraterrestrial construction technologies. Future work will also explore gravity offloading, to simulate the Moon's reduced gravity, as well as testing in a vacuum environment.

ACKNOWLEDGEMENTS

The authors would like to express their sincere gratitude to Kevin Farries and Gary Bowman from Adelaide University for their invaluable support in the design and manufacture of the lunar vibrating drum roller (LVDR-1), and their assistance with laboratory testing. The authors also express their gratitude to the following final year, Civil Engineering Honours students from Adelaide University, who contributed to the testing outlined in this paper: Daniela Jaud, Nicolette Miller, Owen Ong, Tasha Spratling and Lane Whittaker. The authors

also extend their appreciation to Broons Impact Rollers for providing access to the test rig, which was essential for conducting the experimental work. Additionally, the authors acknowledge the facilities and technical support provided by the School of Civil Engineering and Construction Management at Adelaide University. This research was supported in part by institutional resources, and the contributions of all technical staff involved in the experimental setup and data acquisition are gratefully recognised.

REFERENCES

Agarwal, A.K., Scott, B.T., Jaksa, M.B. and Kuo, Y.L., 2026a. Comparison of compaction techniques on lunar highland regolith simulant. *J. Aerosp. Eng.*

Agarwal, A.K., Scott, B.T., and Jaksa, M.B., 2026b. Optimising speed and frequency of a scale model vibrating smooth drum roller on lunar highland regolith simulant. *engrXiv preprint*. https://doi.org/10.31224/6434

Agarwal, A. K., Jaksa, M.B., Scott, B.T. and Kuo, Y.L., 2024. Compaction testing on lunar highland simulant using a vibrating drum roller. In: *Earth and Space 2024: Engineering for Extreme Environments*, 19th ASCE Aerospace Division Biennial International Conference, Miami, FL, USA. https://doi.org/10.1061/9780784485736.068.

Agarwal, A.K., Kuo, Y.L., Jaksa, M.B. and Scott, B.T., 2023. Density, strength and compressibility characteristics of lunar regolith simulant. *engrXiv*. https://doi.org/10.31224/6408.

Bernold, L.E., 1994. Compaction of lunar-type soil. *J. Aerosp. Eng.* 7, 175–187.

Bretreger, A., 2015. Technical Guide L-G-002: Field density testing using a nuclear density gauge. Roads and Maritime Services, NSW Government, Australia.

Carrier, W.D., Olhoeft, G.R. and Mendell, W., 1991. Physical properties of the lunar surface, in: Heiken, G., Vaniman, D. and French, B. (Eds.), *Lunar sourcebook: a user's guide to the Moon*. Cambridge University Press, Cambridge, pp. 475–594.

Das, B. M. and Sobhan, K., 2014. *Principles of geotechnical engineering*, 8th ed., Cengage Learning, Stamford, CT.

Dave, T.N. and Dasaka, S.M., 2011. A review on pressure measurement using earth pressure cell. *Int. J. Earth Sci Eng.* 4(6), 1031–1034.

Dotson, B., Sanchez Valencia, D., Millwater, C., Easter, P., Long-Fox, J., Britt, D. and Metzger, P., 2024. Cohesion and shear strength of compacted lunar and martian regolith simulants. *Icarus*. https://doi.org/10.1016/j.icarus.2024.115943.

Geomil, 2026. D-Cone: digital CPT cone and geotechnical sensor network (GSN). https://www.geomil.com/products/d-cone (accessed January 20, 2026).

Heiken, G. H., Vaniman, D. T. and French, B. M., 1991. *Lunar Sourcebook: A User's Guide to the Moon*, Cambridge University Press, Cambridge, UK.

Humboldt Mfg. Co., 2020. HS-5001SD nuclear density gauge: operating manual. https://www.humboldtmfg.com/manuals/HS-5001SD_MANUAL%20_0920.pdf (accessed 16 January 2026).

Humboldt Mfg. Co., 2026. HS-5001SD nuclear density gauge. https://www.humboldtmfg.com/nuclear-gauge-hs-5001sd.html (accessed 16 January 2026).

Lunne, T., Powell, J.J. and Robertson, P.K., 2002. *Cone penetration testing in geotechnical practice*. CRC Press, Boca Raton, FL, USA. https://doi.org/10.1201/9781482295047.

Massarsch, K.R. and Fellenius, B.H., 2005. Deep vibratory compaction of granular soils. In: *Elsevier Geo-Engineering Book Series*, Vol. 3, pp. 539–561. Elsevier, Amsterdam. https://doi.org/10.1016/S1571-9960(05)80022-9.

Mooney, M.A. and Rinehart, R.V., 2009. In situ soil response to vibratory loading and its relationship to roller-measured soil stiffness. *J. Geotech. Geoenviron. Eng.* 135(8), 1022–1031. https://doi.org/10.1061/(ASCE)GT.1943-5606.0000046.

Richart, F.E., Hall, J.R. and Woods, R.D., 1970. *Vibrations of soils and foundations*. Prentice-Hall, Englewood Cliffs, NJ.

Rinehart, R.V. and Mooney M.A., 2009. Measurement of roller compactor induced triaxial soil stresses and strains. *Geotech. Test. J.* 32(4), 347–357. https://doi.org/10.1520/GTJ101889.

Robertson, P.K., 2009. Interpretation of cone penetration tests—a unified approach. *Can. Geotech. J.* 46(11), 1337–1355. https://doi.org/10.1139/T09-065.

Space Resources Technologies, 2021. *Exolith lab LHS-1E Lunar Highlands Simulant: Fact Sheet 001-09-001-0120.* https://cdn.shopify.com/s/files/1/0398/9268/0862/files/lhs-1E-spec-sheet-2021.pptx_1.pdf?v=1693316297 (accessed 16 January 2026).

Scott, B., Jaksa, M. and Mitchell, P. 2019. Ground response to rolling dynamic compaction. *Geotech. Lett.* 9(2), 99–105. https://doi.org/10.1680/jgele.18.00208.

Scott, B.T., Kuo, Y.L., Jaksa, M.B. and Agarwal, A.K. 2023. Compaction trial on lunar regolith simulant. *engrXiv*. https://doi.org/10.31224/6410.

Slabic, A., Gruener, J.E., Kovtun, R.N., Rickman, D.L., Sibille, L., Oravec, H.A., Edmunson, J. and Keprta, S., 2024. Lunar regolith simulant user's guide, Rev. A. NASA/TM-20240011783, National Aeronautics and Space Administration, Washington, DC. https://ntrs.nasa.gov/api/citations/20240011783/downloads/Lunar_Regolith_Simulant_Users_Guide_Rev_A_28OCT.pdf (accessed 16 March 2026).

Standards Australia, 1998. *Methods of testing soils for engineering purposes - Soil compaction and density tests - Determination of the minimum and maximum dry density of a cohesionless material (AS 1289.5.5.1).* Standards Australia, Sydney, Australia.

Standards Australia, 1999. *Methods of testing soils for engineering purposes - Soil compaction and density tests - Determination of the static cone penetration resistance of a soil - Field test using a mechanical and electrical cone or friction-cone penetrometer (AS 1289.6.3.1).* Standards Australia, Sydney, Australia.

Standards Australia, 2007. *Methods of testing soils for engineering purposes - Soil compaction and density tests - Determination of field density and field moisture content of a soil using a nuclear surface moisture-density gauge – Direct transmission mode (AS 1289.5.8.1).* Standards Australia, Sydney, Australia.

Terzaghi, K., Peck, R.B. and Mesri, G., 1996. *Soil mechanics in engineering practice*, 3rd ed. John Wiley & Sons, New York.

Toklu, Y.C. and Akpinar, P., 2022. Lunar soils, simulants and lunar construction materials: An overview. *Adv. Space Res.* 70(3), 762–779. https://doi.org/10.1016/j.asr.2022.05.017 .

Wersäll, C., 2016. *Frequency optimization of vibratory rollers and plates for compaction of granular soil*. PhD dissertation, KTH Royal Institute of Technology, Stockholm, Sweden.